

The Gaia-ESO Survey: No sign of multiple stellar populations in open clusters from their sodium and oxygen abundances^{*}

A. Bragaglia¹, V. D'Orazi^{2,3}, L. Magrini⁴, M. Baratella⁵, T. Bensby⁶, S.L. Martell^{7,8}, S. Randich⁴, G. Tautvaišienė⁹, E. J. Alfaro¹⁰, L. Morbidelli⁴, R. Smiljanic¹¹, and S. Zaggia²

¹ INAF-Osservatorio di Astrofisica e Scienza dello Spazio di Bologna, via P. Gobetti 93/3, 40129, Bologna, Italy
e-mail: angela.bragaglia@inaf.it

² INAF-Osservatorio Astronomico di Padova, vicolo dell'Osservatorio 5, 35122, Padova, Italy

³ Dipartimento di Fisica, Università degli Studi di Roma Tor Vergata, via della Ricerca Scientifica 1, 00133, Roma, Italy

⁴ INAF-Osservatorio Astrofisico di Arcetri, largo E. Fermi 5, 50125, Firenze, Italy

⁵ European Southern Observatory, Alonso de Córdova 3107, Vitacura, Santiago, Chile

⁶ Lund Observatory, Division of Astrophysics, Department of Physics, Lund University, Box 118, SE-22100 Lund, Sweden

⁷ School of Physics, University of New South Wales, Sydney, NSW 2052, Australia

⁸ Centre of Excellence for Astrophysics in Three Dimensions (ASTRO-3D), Australia

⁹ Institute of Theoretical Physics and Astronomy, Vilnius University, Saulėtekio av. 3, LT-10257 Vilnius, Lithuania

¹⁰ Instituto de Astrofísica de Andalucía-CSIC, Apdo. 3004, 18080, Granada, Spain

¹¹ Nicolaus Copernicus Astronomical Center, Polish Academy of Sciences, ul. Bartycka 18, 00-716, Warsaw, Poland

June 12, 2024

ABSTRACT

Context. The light element (anti-)correlations shown by globular clusters (GCs) are the main spectroscopic signature of multiple stellar populations. These internal abundance variations provide us with fundamental constraints on the formation mechanism of stellar clusters.

Aims. Using *Gaia*-ESO, the largest and most homogeneous survey of open clusters (OCs), we intend to check whether these stellar aggregates display the same patterns. Based on previous studies of many GCs, several young and massive clusters in the Magellanic Clouds, as well as a few OCs, we do not expect to find any anti-correlation, given the low mass of Milky Way OCs.

Methods. We used the results based on UVES spectra of stars in *Gaia*-ESO to derive the distribution of Na and O abundances and see whether they show an unexplained dispersion or whether they are anti-correlated. By selecting only high-probability members with high-precision stellar parameters, we ended up with more than 700 stars in 74 OCs. We examined the O-Na distribution in 28 OCs with at least 4 stars available as well as the Na distribution in 24 OCs, with at least 10 stars available.

Results. We find that the distribution of Na abundances is compatible with a single-value population, within the errors. The few apparent exceptions can be explained by differences in the evolutionary phase (main sequence and giant post first dredge-up episode) or by difficulties in analysing low gravity giants. We did not find any indication of an Na-O anti-correlation in any of the clusters for which O has been derived.

Conclusions. Based on the very small spread we find, OCs maintain the status of single stellar populations. However, a definitive answer requires studying more elements and larger samples covering different evolutionary phases. This will be possible with the next generation of large surveys.

Key words. stars: abundances – stars: kinematics and dynamics – (Galaxy) open clusters and associations: general – techniques: radial velocities – techniques: spectroscopy

1. Introduction

Stellar clusters could serve as the best exemplification of a simple stellar population, since they are composed of stars of different masses that were born together and characterised by the same age and initial chemical composition. Thus, they offer an optimal way to study stellar and galactic evolution, representing ideal benchmarks. However, this simple view (see Renzini & Fusi Pecci 1988, to cite only one historical review) had to be abandoned in the case of globular clusters (GCs). Starting

from low-resolution spectroscopy indicating anti-correlated star-to-star variation in CN and CH (e.g. Smith & Norris 1993) and from the high-resolution works by the Lick-Texas group (e.g. Kraft et al. 1993), evidence has mounted to suggest that stars in GCs display light element abundances (in particular, O, Na, Mg, and Al), which are vastly different from those of field stars of similar metallicity (see e.g. Gratton et al. 2000, 2001, for low-metallicity field stars and GCs). The new paradigm for GCs is that they are composed by multiple populations, as described, for instance, in recent reviews by Gratton et al. (2012, 2019); Bastian & Lardo (2018). This is important when seeking to understand how GCs form. The question of whether 'multiple' also points to different ages (as suggested by most models of early

^{*} Based on observations collected at the ESO telescopes under programme 188.B3002, 193.B-0936, and 197.B-1074, the *Gaia*-ESO Public Spectroscopic Survey.

chemical enrichment) is still a matter of debate. What is clear is that stars of very different chemical compositions (with respect to proton-capture elements and helium) coexist in the same GC. This is amply seen in photometry as well, especially when combinations of filters sensitive to light element variations are used (as in the works using Johnson, Strömgren, or Hubble Space Telescope UV filters, see e.g. Monelli et al. 2013; Carretta et al. 2011; Milone et al. 2017). Initially, only GCs in the Milky Way (MW, all very old, see e.g. Kruijssen et al. 2019) had been studied in the past, followed by massive clusters in nearby galaxies, such as the Magellanic Clouds later on (e.g. Mucciarelli et al. 2009). Light-element variations were searched for via spectroscopic or photometric means and were indeed found in (massive) clusters down to an age of 2 Gyr (e.g. Martocchia et al. 2019; Oh et al. 2023).

Interestingly, light-element (anti-)correlations have been found for all MW GCs examined (Bastian & Lardo 2018; Gratton et al. 2019), possibly with the exception of Ruprecht 106 (Freljij et al. 2021); however, this is not the case for open clusters (OCs). These younger, less massive, and more metal-rich stellar clusters have not been extensively studied in this context. As far as we know, only two old and massive OCs (i.e. Berkeley 39 and NGC 6791) have been observed on purpose with high-resolution spectroscopy to see whether they host multiple populations. Bragaglia et al. (2012, 2014) and Villanova et al. (2018) examined some tens of giant stars in these two OCs, looking for variations in light elements, but did not find any evidence of them. Literature studies on OCs do not usually have large samples and are not focussed on this subject, but generally no evidence has been found either, as seen in the discussion in MacLean et al. (2015). There is one exception, however: Pancino 2018 collected literature data on four nearby intermediate-age OCs and found indication of variations in Na, O, and Mg among main sequence stars that are similar to those seen for GCs. None of these four OCs has a mass comparable to that of GCs, indicating that we cannot safely exclude OCs only because of their low mass. The features are enhanced in fast-rotating massive stars ($v \sin i > 50 \text{ km s}^{-1}$). These authors noted that these anomalous abundances would not survive the first dredge-up, thus disappearing in giants.

Indeed, the first dredge-up plays a role in Na abundances, which may be increased after it in young clusters. Stellar evolutionary models, for instance by Lagarde et al. (2012), indicate an enhancement in stars with mass larger than about $2 M_{\odot}$ at the main sequence turn-off. This has been confirmed by observations of open clusters and Cepheids, both within GES and in additional samples, see Smiljanic et al. (2016, 2018) for more details. This point will be discussed later in our paper for the few OCs with both dwarf and giant stars observed.

All this calls for further analysis, involving both dwarf and giant stars. Luckily, the paucity of studies on multiple populations in OCs may now be amended using the large data set produced by *Gaia*-ESO (GES hereinafter). *Gaia*-ESO is a public spectroscopic survey conducted with FLAMES at the ESO VLT¹ over 340 nights from December 2011 to January 2018. A full description of the survey goals and strategy can be found in Gilmore et al. (2022); Randich et al. (2022). Briefly, GES ob-

served about 115000 stars in the thin and thick disc, bulge, and halo of the Milky Way. It dedicated a large fraction (about 37%, see Randich et al. 2022) of the time to OCs and star-forming regions. For a description of goals, main results, and selection process, we refer to Randich et al. (2022); Bragaglia et al. (2022). In total, 62 stellar clusters were observed by GES for science and a handful for calibration (Pancino et al. 2017b). Then, data for 18 further OCs were retrieved from the ESO archive (mostly UVES spectra). A complete list with main properties can be found in Randich et al. (2022) and in Table A.1. In each cluster, GES obtained spectra of stars in all evolutionary phases (from about 100 to more than 1000 stars). Bragaglia et al. (2022) describes the cluster types, the observational strategy, and the kind of targets observed.

All spectra are available from the ESO archive (both raw and science-ready spectra) online². A catalogue containing radial and projected rotational velocities, stellar parameters (effective temperature, surface gravity and metallicity), abundances of many elements, parameters for tracing accretion and activity in young stars, etc. can be found at the ESO Catalogue website.³

In the present paper, we describe the data used in Sect. 2, along with the the Na and O distributions in Sect. 3, where we also discuss some clusters. A summary and conclusion are provided in Sect. 4, while additional information on the clusters and individual targets is given in Appendix.

2. The data

We used the GES final, public catalogue and selected only the observations in the OC fields, using the field GES_FLD, which contains the name of the clusters. We then cross-matched the selected stars with *Gaia* EDR3 (*Gaia* Collaboration et al. 2021) using the TOPCAT table access protocol and a search radius of 2 arcsec. After the *Gaia* DR3 release (*Gaia* Collaboration et al. 2023), we added also the radial velocity (RV) information. The match resulted in 42776 stars, but only part of them actually cluster members, as reported, for instance, in Bragaglia et al. (2022) and Jackson et al. (2022) for some statistics on membership. To select only high probability members we used Cantat-Gaudin et al. (2020, based on *Gaia* DR2 astrometry) and Jackson et al. (2022, which also includes information from GES, such as RV, temperature, and so on in addition to *Gaia* EDR3 astrometry). Keeping only stars with a probability larger than 0.7 in at least one of the two studies, we obtained about 14000 stars.

As we were interested in the abundances of Na and O, we further selected only stars observed with UVES (at a resolution of 47000). In particular, we kept only stars observed with the U580 setup, covering the 4800-6000 Å region. The main GIRAFFE setups used for the OCs (HR15n and HR09b, see Bragaglia et al. 2022; Randich et al. 2022) do not contain lines of either element⁴. This selection drastically reduced our sample to 970 stars. Finally, we applied quality cuts similar to what was done in other GES papers and kept only stars for which errors

² <http://archive.eso.org/cms.html>

³ (<https://www.eso.org/qi/catalogQuery/index/393>)

⁴ We did not consider Mg and Al, also available from the GIRAFFE spectra, because they are not known to vary as much as O, Na in metal-rich GCs. Indeed, the production of Al is larger in the metal-poorer and more massive GCs, as first noted by Carretta et al. (2009a) and later confirmed on larger samples, a metallicity that is well below and a mass well above that of OCs.

¹ ESO stands for European Southern Observatory, VLT for Very Large Telescope, FLAMES for Fibre Large Array Multi Element Spectrograph (described in Pasquini et al. 2002). FLAMES has two spectrographs, UVES (Ultraviolet and Visual Echelle Spectrograph, Dekker et al. 2000) at resolution $R \sim 45000$ and GIRAFFE, at intermediate resolution ($R \sim 20000$, depending on the setup).

on temperature, gravity, and metallicity were less than 100 K, 0.3 dex, and 0.1 dex, respectively (all three conditions met).

The only available O lines were the [O I] transitions at 6300 and 6363 Å, more easily measured in giants than in dwarfs. Correction for telluric lines was not part of the standard GES processing (see Sacco et al. 2014, for the UVES spectra). This means that oxygen abundance was measured from the [O I] 6300 Å line only in part of the clusters when the combination of intrinsic line of sight (LoS) velocity and barycentric motion kept the line free from contamination. We indicate in Table A.1 the cases for which O was measured and for which we could hope to explore the existence of a Na-O anti-correlation (however, see the limitations imposed on precision and the minimum number of stars; for instance, in IC 2602 we have 18 stars, but O was measured only in one).

A detailed description of how UVES spectra are reduced and stellar parameters and abundances are computed in GES can be found in Sacco et al. (2014); Smiljanic et al. (2014); Randich et al. (2022); Gilmore et al. (2022). Briefly, after data reduction, the spectra are analysed by multiple pipelines and astrophysical parameters are internally homogenised within each working group (WG; here, WG 11, dealing with UVES spectra). A second homogenisation process, involving results of all WGs and based on a set of calibrators (benchmark stars, OCs, and GCs; see Pancino et al. 2017a) produces the set of recommended parameters published in the released catalogue. Abundances from UVES spectra are then computed by each analysis node with the homogenised stellar parameters. The abundances from the different nodes are combined line by line with a Bayesian approach by WG 11 (see Worley et al. 2024 for the updated description of the WG 11 approach). The abundances of O, C, and N (the last two from molecular bands) are an exception since they are measured only by the Vilnius analysis node. Finally, the final abundances are released by WG 15, dedicated to quality control, homogenisation, and preparation of the final catalogue.

Abundances in GES were calculated assuming local thermodynamic equilibrium (LTE) approximation. Ideally, a correction should be applied to non-LTE (NLTE), which offers a better description. Indeed, NLTE corrections depend on many factors (in particular on temperature and gravity) and avoiding them may skew the distribution of abundances. However, given the way the GES abundances are calculated (see Smiljanic et al. 2014; Gilmore et al. 2022; Randich et al. 2022), this is complicated and we keep to the LTE values. This is irrelevant for O, measured essentially only in giants (most are red clump, RC, stars) from a forbidden line, that is, not subject to NLTE effects (Asplund et al. 2004). For Na, we minimise the effects by separating dwarfs and giants, thus considering samples with less disparate parameters.

The final sample contains 735 stars in 84 clusters, 74 of which have at least three stars (the number of stars surviving all cuts varies from one to 68). We give information on stellar parameters, RV, and selected abundances for the total selected sample in Table A.2. We have both O and Na abundances for 270 stars; 240 of them are in 28 OCs with at least 4 stars available, while 22 OCs have only one to three stars. Sodium is measured essentially in all stars and there are 24 OCs with at least ten stars with Na abundance.

3. The Na and O distribution in GES OCs

3.1. Considering O and Na

In Fig. 1, we show the distribution of O and Na abundances in the 28 OC, individually and all together. We use [O/H] and [Na/H] to avoid introducing the effect of [Fe/H], which shows a bland dependence on temperature and gravity (a discussion, employing OC data, is presented in Magrini et al. 2023). The effect could mask or introduce spreads when stars of very different parameters are considered in the same cluster (a few cases are discussed in Sect. 3.3). However, we show in Appendix (Sect. A.2) that using [O/Fe] and [Na/Fe] does not change our conclusions.

We also compared the distribution(s) to that of the GC 47 Tuc, analysed by GES in a homogeneous way. This cluster was chosen because it is a metal-rich GC showing a "short" anti-correlation (see Carretta et al. 2009b,a for a comparison to other globulars). As we see from the right-most lower panel of Fig. 1, there is a different (minimum) value for Na and (maximum) value for O in the OCs, which are a thin-disk, relatively young population, and in the GC. This is evident also in Fig. A.1, where we see that 47 Tuc has the typical high $[\alpha/\text{Fe}]$ abundance ratio of the old stellar populations. In fact the [O/Fe] values of the 47 Tuc stars of primordial composition (high O and low Na) are larger than for OC stars.

Crucially, we do not see an indication of anti-correlation between O and Na in any of the OCs in Fig. 1. Either the distributions are compatible with a dispersion due to errors (in NGC 6005, Tr 23, Be 39, etc.), or we see a correlation (in NGC 2243, NGC 6259, NGC 6705, etc.), which is however not significant. Based on these data, OCs should be considered basically different from GCs.

However, the evidence against OCs hosting multiple populations may still be considered not conclusive. First, we can address the issue in about one-third of the whole GES sample because O was measured only in a fraction of the clusters. Second, we have only six clusters with at least 10 stars with both abundances, at variance with the dedicated studies on NGC 6791 and Be 39 mentioned in the introduction (35 stars in Bragaglia et al. 2014 and 17 in Villanova et al. 2018 for the first, and 29 in Bragaglia et al. 2012 in the latter). In addition, the extension of the O-Na anti-correlation shows a dependence on cluster mass in GCs, see the measure of the inter-quartile ratio (IQR) of [O/Na] (see Carretta et al. 2010; Gratton et al. 2019 for examples). Open clusters have generally (much) lower masses than GCs (see e.g. Fig. 7 in Gratton et al. 2019); a simple linear extrapolation of the relation between mass and IQR[O/Na] would lead to very small (even negative) values. For a direct comparison of total masses, see for instance Baumgardt & Hilker (2018) for GCs (updated online⁵), with values about $10^3 - 10^6 M_{\odot}$ and Ebrahimi et al. (2022); Almeida et al. (2023) for 15 OCs and more than 700 OCs, respectively, with a few hundreds to a few thousands M_{\odot} . In Table A.1 we indicate the masses of the 23 GES OCs which are present in these two sources.

3.2. Considering only Na

We can also look at Na alone to check whether a significant star-to-star variation exists. This permits us to include a few clusters for which no, or very few, O measures are available (NGC 2420, NGC 3532, NGC 2514, NGC 2425, Tr 20, Be 81, and Blanco 1

⁵ <https://people.smp.uq.edu.au/HolgerBaumgardt/globular/>

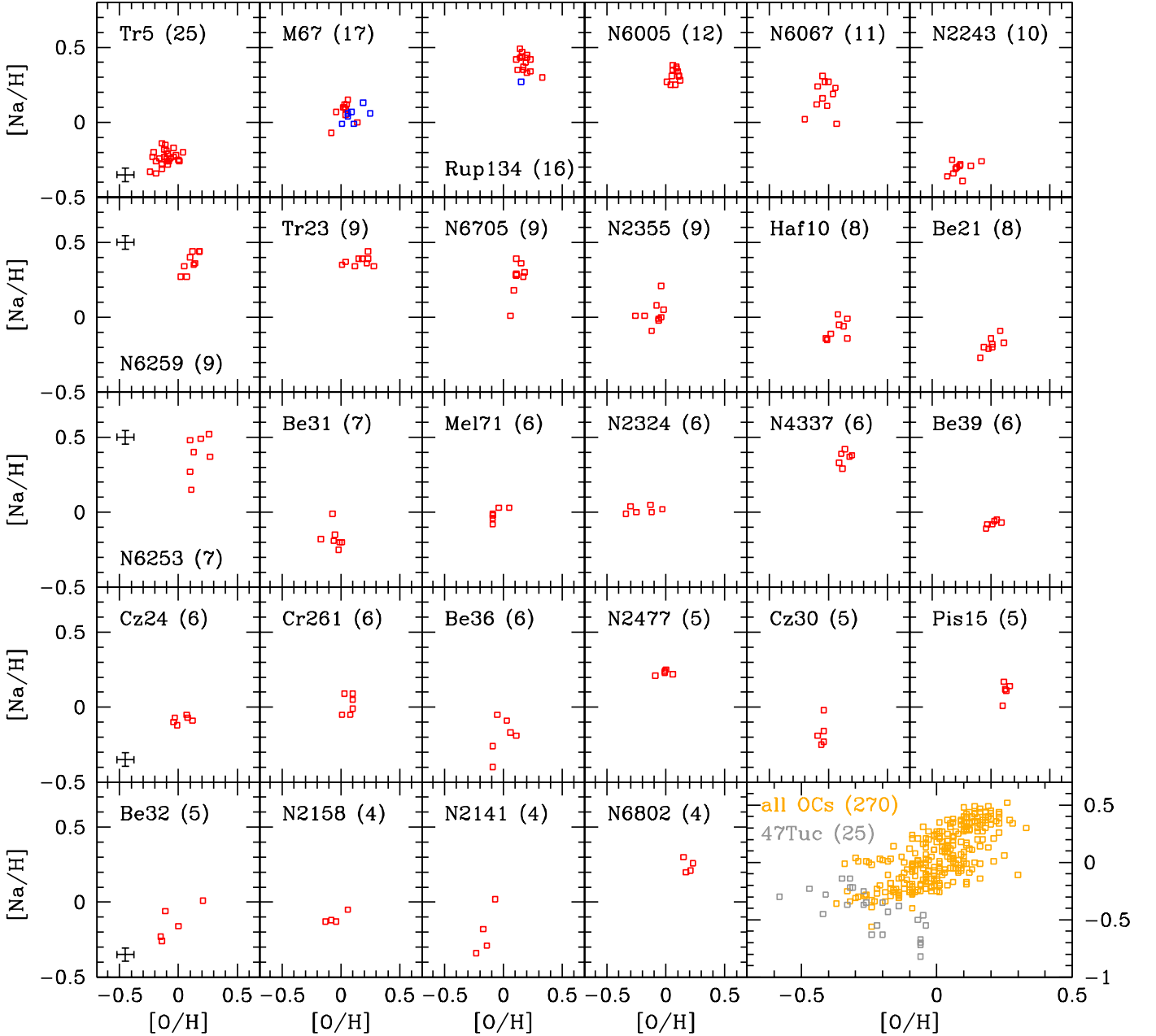


Fig. 1. Distribution of $[\text{Na}/\text{H}]$ versus $[\text{O}/\text{H}]$ for all OCs with at least four stars with valid values. The blue points for two clusters indicate dwarf stars, while all red points are for giants. The bottom right panel displays the available values in all OCs (in orange) compared to the GC 47 Tuc (grey points). Average error bars are displayed only in the first column of the plots.

are in the first category, NGC 2141, NGC 2158, NGC 2477, NGC 6802, and Be 32 in the second). This is apparent from the comparison of Figs. 1 and 2. In the latter, we only plot the $[\text{Na}/\text{H}]$ histograms of OCs with at least ten valid measurements. The analogous plot involving $[\text{Na}/\text{Fe}]$ is shown in Fig. A.2. In Fig. 2 we also plot the histogram of $[\text{Na}/\text{H}]$ values in 47 Tuc in each panel for immediate comparison: apart from a different zero point (see Fig. A.2, where the metallicity is taken into account), the distribution of all OCs is always much narrower (about two to six times narrower, judging from Table 1). For the OCs, we separated dwarfs on the main sequence (MS) and giants by selecting stars with $\log g$ larger or smaller than 3.5, respectively.

This allowed us to avoid seeing the effect of evolution on Na abundance (see Sect. 3.3) and also to minimise possible differences due to LTE assumptions (see Sect. 2).

Table 1 lists the 24 resulting OCs and gives information on the number of stars, the mean $[\text{Na}/\text{H}]$ values together with standard deviations, median and the $\text{IQR}([\text{Na}/\text{H}])$ values. The mean $[\text{Na}/\text{H}]$ and its intrinsic dispersion (cols. 5-6) have been computed using a maximum likelihood algorithm (kindly made available by the authors), which takes into account also the errors, better computing the intrinsic dispersion (for details, see Mucciarelli et al. 2012). For comparison, we list the same values for 47 Tuc. In Fig. 3, we plot the median values for the 24

Table 1. Information on mean [Na/H], dispersion and IQR([Na/H]) for GES OCs and 47 Tuc.

Ord	Cluster	Age (Gyr)	Num	mean [Na/H]	sigma	median [Na/H]	median [Fe/H]	IQR [Na/H]
1	NGC 6253	3.24	68	0.478	0.099	0.38	0.36	0.13
2	M 67	4.27	38	0.040	0.054	0.05	-0.02	0.10
3	NGC 3532	0.40	36	0.000	0.078	-0.02	-0.01	0.12
4	Trumpler 5	4.27	26	-0.245	0.038	-0.23	-0.35	0.06
5	NGC 2141	1.86	23	0.004	0.064	0.01	-0.05	0.09
6	Ruprecht 134	1.66	20	0.399	0.045	0.41	0.27	0.09
7	Trumpler 20	1.86	26	0.184	0.041	0.17	0.13	0.08
8	NGC 2243	4.37	18	-0.279	0.041	-0.28	-0.47	0.06
9	Berkeley 32	4.90	17	-0.141	0.085	-0.16	-0.29	0.12
10	NGC 2516	0.24	15	-0.039	0.051	-0.05	-0.05	0.08
11	NGC 2158	1.55	14	-0.076	0.038	-0.05	-0.16	0.09
12	NGC 2425	2.40	14	-0.059	0.066	-0.07	-0.14	0.12
13	NGC 6067	0.13	13	0.216	0.141	0.23	-0.03	0.15
14	Berkeley 21	2.14	13	-0.204	0.068	-0.20	-0.21	0.06
15	NGC 6005	1.26	13	0.343	0.018	0.31	0.22	0.08
16	Berkeley 81	1.15	13	0.348	0.057	0.36	0.25	0.14
17	NGC 6259	0.34	12	0.379	0.045	0.38	0.17	0.10
18	Haffner 10	3.80	12	-0.079	0.047	-0.07	-0.12	0.10
19	NGC 2477	1.12	11	0.156	0.072	0.21	0.13	0.15
20	Trumpler 23	0.71	11	0.346	0.079	0.37	0.21	0.04
21	Blanco 1	0.10	11	-0.083	0.065	-0.07	-0.05	0.09
22	NGC 2420	1.74	37	-0.098	0.088	-0.08	-0.16	0.11
23	NGC 6705	0.31	10	0.282	0.023	0.28	0.06	0.04
24	NGC 6802	0.66	10	0.269	0.029	0.27	0.15	0.06
25	47 Tuc (GC)		66	-0.44	0.20	-0.43	-0.75	0.30

Notes. 'Ord' is the index used in Fig. 3 on the x-axis to indicate the cluster; 'Num' indicates how many stars were used to compute the mean, dispersion, and median [Na/H]; the last column shows IQR([Na/H]), that is the difference between the 3rd and 1st quartiles of the [Na/H] distribution.

OCs, together with the extension of the variation (the lines show the first and third quartile of the [Na/Fe] distributions). The extensions are always small, see the comparison with 47 Tuc, also shown in the figure. As the number of star with Na abundance is larger than in the OCs, with the exception of NGC 6253, we tested the effect of having only a small number of stars on the IQR. Figure 4 shows the distribution of IQR[Na/H], when only 10 stars are randomly extracted from the 47 Tuc sample (we selected 10 as this is the smallest number of stars for which we measured IQR in GES OCs). The random extraction was repeated 10000 times and we measured an IQR[Na/H] larger than 0.15, that is, the highest value found for OCs, in 85% of the times.

Also, when using only the Na abundances, we did not see any indication of large star-to-star variation. In particular, we do not see any unexpected Na enhancement (see also Sect. 3.3) similar to that seen in GCs. No clear evidence of multiple populations is found, although given the differences in age and mass, the results are inconclusive as to whether multiple populations are actually present.

As a sanity check, we considered two non-GES sets of data of comparable size. First, we took the eleven giant stars in NGC 6705 analysed in Loaiza-Tacuri et al. (2023); these authors used the BACCHUS code on APOGEE spectra and derived abundances of many elements (including Na). The mean and intrinsic dispersion of [Na/H], computed as for the GES data, are +0.46 (assuming 6.18 as solar value) and 0.039. While the Na abundance is clearly different from the GES value, the dispersion

is comparable and compatible with their errors. Second, we took Stock 2, a cluster where both dwarfs and giants were observed by the SPA large programme at the TNG using the very-high-resolution spectrograph HARPS-N (see Alonso-Santiago et al. 2021, who estimated an age of about 0.5 Gyr). For Stock 2, there are Na abundances for 10 giants and 12 main sequence stars. If we consider them together we have a mean [Na/H] of +0.145 with sigma 0.052, similar to what we get for GES clusters. When we split the sample between dwarfs and giants we get averages of 0.217 and 0.07, respectively, with an essentially zero intrinsic dispersion. While the dispersion is always small, we see that it is safer to separate dwarfs from giants in clusters young enough to display an enhanced Na abundance after the first dredge-up. That means clusters with mass at the turn-off larger than $2 M_{\odot}$, according to Smiljanic et al. 2016, 2018. For the GES OCs in Table 1, this may affect only NGC 3532 and NGC 2477, both discussed in Sect. 3.3.

3.3. Some odd cases

Using the [O/Fe] and [Na/Fe] values, a larger than expected variation in the O-Na or Na distribution is visible in a few OCs (see Figs. A.1, A.2, and Table A.2). In other OCs, only one star de-

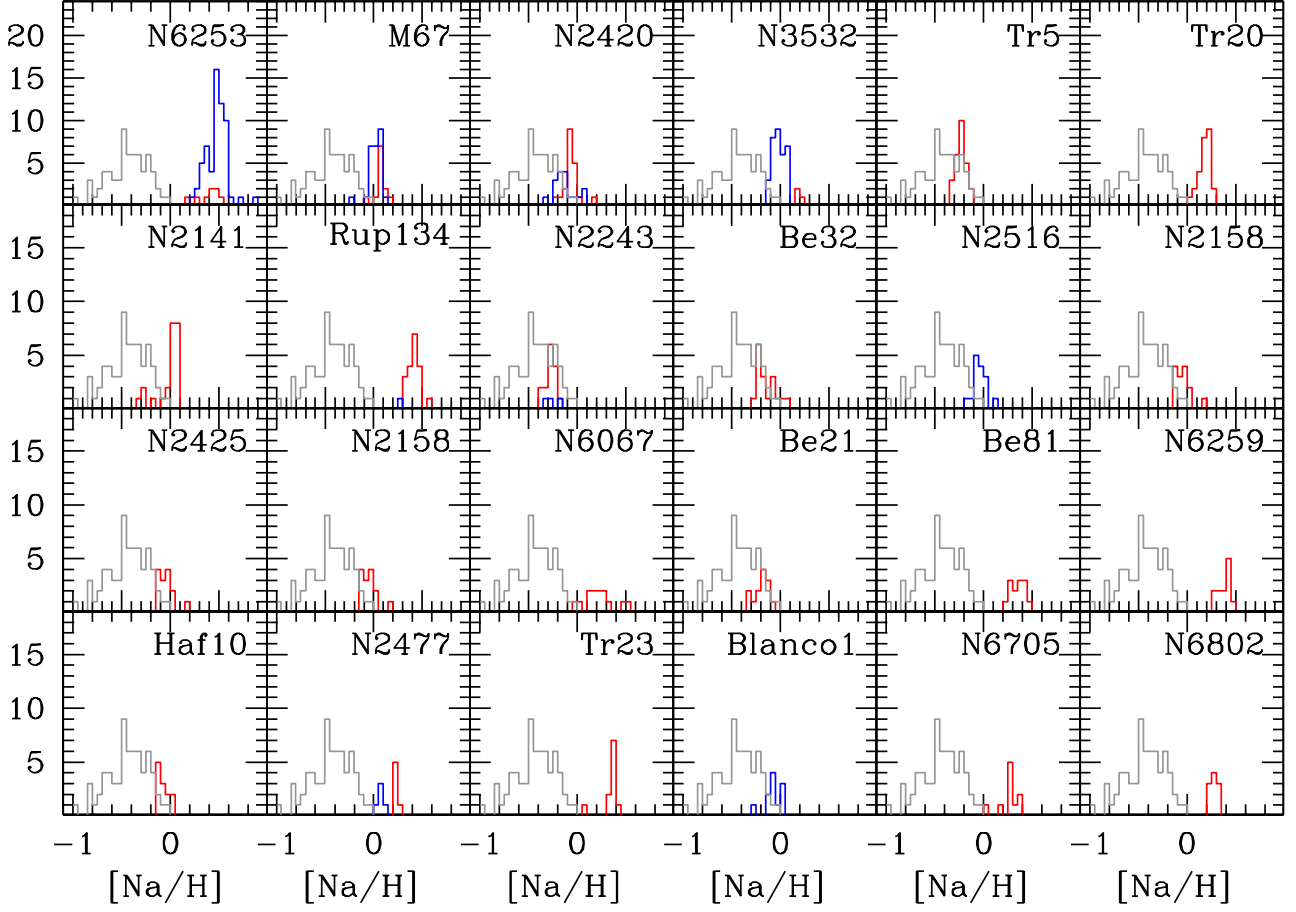


Fig. 2. Histogram of $[Na/H]$ for all OCs with at least ten stars with valid values. The blue histograms are drawn for dwarfs and the red histograms for giants in each cluster, respectively. The histogram for 47 Tuc (grey histogram) is also shown in each panel for comparison.

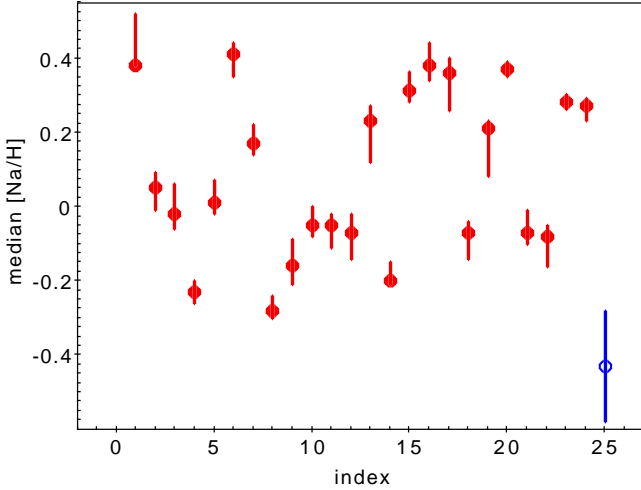


Fig. 3. Median value of $[Na/H]$ for OCs with at least ten valid Na values; the vertical lines indicate the first and third quartile of the distribution in each cluster, that is, the IQR for $[Na/H]$. The rightmost point (blue open circle) is for 47 Tuc. The value of index identifying each OC can be found in Table. 1

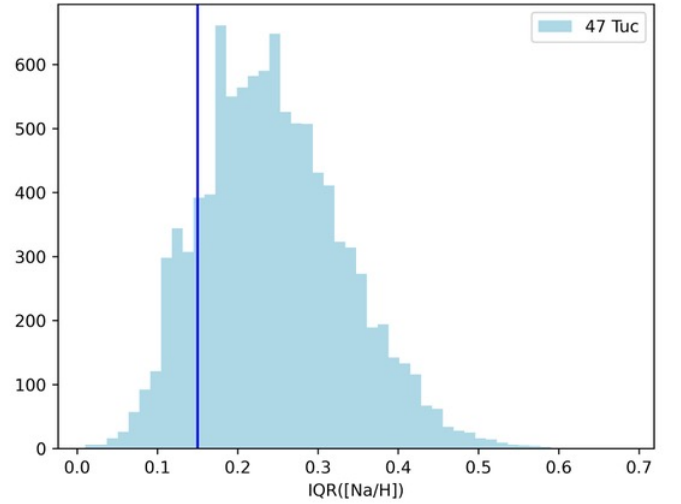


Fig. 4. Histogram of the $IQR([Na/H])$ values for 47 Tuc if only 10 stars are randomly selected among those included in GES. We did 10000 realisations of the IQR and we obtain a value larger than the largest for OCs (0.15, indicated by the vertical line) in 85 % of the cases.

viates from the bulk distribution in each cluster.⁶ We discuss some exemplary cases below.

⁶ While checking these stars, we made use also of the RV in *Gaia* DR3, finding that many stars are candidate or confirmed binary sys-

tems. We present a comparison of GES and GDR3 velocities, indicating discrepant cases, in the appendix (Sect.A.4)

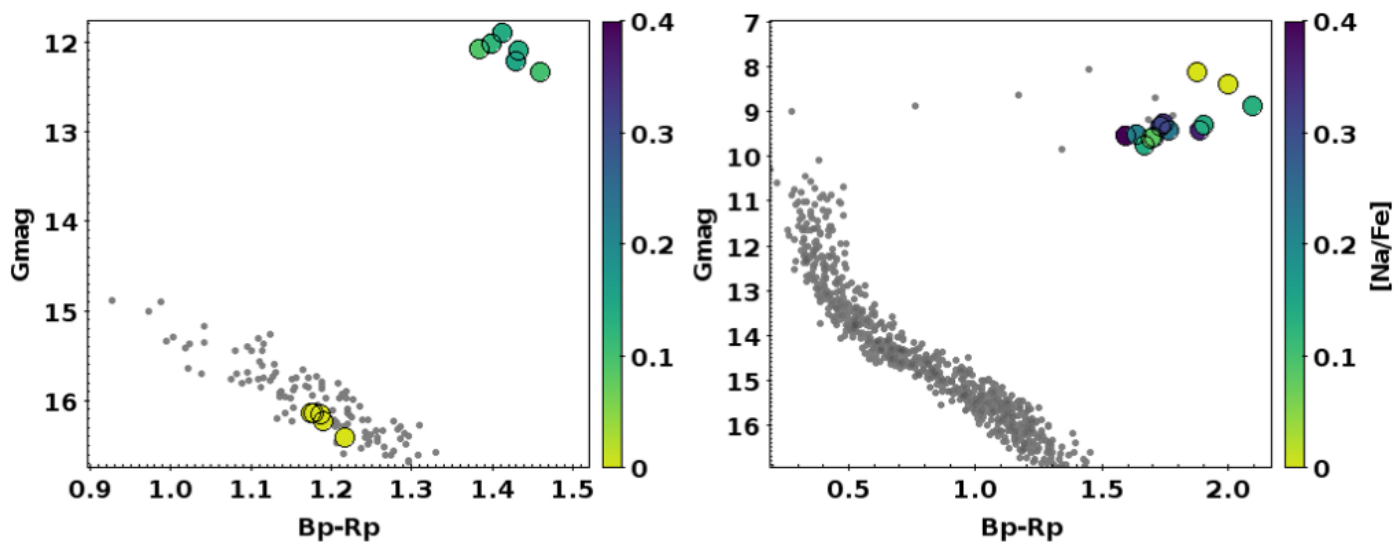


Fig. 5. Colour-magnitude diagrams for NGC 2477 (left) and NGC 6067 (right), drawn using *Gaia* photometry of stars observed by GES. Stars with valid Na abundances are shown as larger symbols, coloured according to their $[Na/Fe]$ value.

NGC 2477 - This is one of the few clusters where both MS and giant stars were observed. At its age (about 1 Gyr, see Table A.1), we expect to see some Na enhancement in giants past the first dredge-up, see Smiljanic et al. (2016, 2018). Also looking at Fig. 2, dwarfs and giants have separated distribution in $[Na/H]$. Indeed, as we see from Fig. 5, left panel, the stars with higher Na content are all located on the RC, and those with lower Na are all on the MS (as in the case of Stock 2, discussed above). Stars within each group have very similar Na abundance, while there is an offset of about 0.2 dex in $[Na/Fe]$ between MS and RC stars. For NGC 2477, the larger Na dispersion is then due to an evolutionary phenomenon. Note that in older clusters, such as M67 and NGC 2243, where we do not expect Na mixing at the first dredge-up, we do not see a difference in the Na abundances of MS and giant stars.

NGC 3532 - The cluster has an age of ≈ 400 Myr and also in this case both MS and giant stars were observed (34 and three valid $[Na/Fe]$ values, respectively). Again, the average $[Na/Fe]$ abundances differ by about 0.2 dex, with giants having larger Na abundance. We conclude that also in this case we are looking at an evolutionary effect (which we should expect whenever the cluster is younger than about 1 Gyr and has a turn-off mass larger than about $2 M_{\odot}$; see Fig. 2 in Smiljanic et al. 2018)

NGC 6067 - In this cluster (age 125 Myr), all stars observed with UVES are giants (see right panel of Fig. 5). However, given the young age, all of them have very low gravity ($\log g$ from 0.7 to 1.8) The analysis of low-gravity stars is problematic, as discussed at length in the GES paper dealing with abundance gradients based on OCs (Magrini et al. 2023, to which we refer to find other OCs and stars affected). In this case, the larger dispersion in Na (confirmed also for other elements, such as Al, Mg, Si, Ca, Ti I, at 0.17, 0.10, 0.14, 0.14, and 0.21 dex, respectively) seems to be due to analysis issues and not to an intrinsic difference in abundance values.

Individual cases - There are some stars with high $[Na/Fe]$ compared to the cluster average. One is in Mel 71 (*Gaia* DR3 ID 3033958747506151424), which has $[Na/Fe]=+0.44$ (compared to an average value of +0.11 of the other stars, while O is not measured). However, its Na abundance seems in line with the other elements, the effect is due to its low metallicity ($[Fe/H]=-0.39$, compared to -0.12). The star is a binary (it is MMU 29 in Mermilliod et al. 2008), also confirmed by the RV difference between GES and GDR3. Another one is in M67 (*Gaia* DR3 604922985178465152). In this case, $[Na/Fe]=+0.30$ (compared to an average value of +0.06 without it) and again the star has a Na abundance similar to the others, no measurement of O, a lower than average metallicity, and is a binary based on the RV difference between GES and GDR3. In both cases, the stars are very high probability astrometric members.

There are also stars with $[Na/Fe]$ values much lower than the cluster average. Two cases are star *Gaia* DR3 3029944366134389888 in NGC 2425 and star *Gaia* DR3 2893944295419313280 in NGC 2243 (neither has O measured). The first is a low-gravity star (see the caveat on the difficulties in their analysis) and is probably a binary, the second has a discrepant metallicity ($[Fe/H]=-0.15$ dex, higher than the cluster average, see Table 1). Finally, the lowest $[Na/Fe]$ star in NGC 6067 (*Gaia* DR3 5932570607366776960), actually has the highest $[Na/H]$; however, although the star passed the quality cuts and is a member both according to its RV and astrometry, its $[Fe/H]$, at +0.5 dex compared to a median of -0.03 dex (Table 3), indicates possible problems in the analysis.

In conclusion, these high-probability cluster members seem to be a mixed bag of discrepant objects. In some cases, we are dealing with binaries and their metallicities and abundances may be lower due to veiling from a secondary component. In others, their low gravity may explain the discrepancies. While they surely merit being checked, further attention is not required for the main goal of our paper.

4. Summary and conclusions

We used the public survey GES to study the possible presence of star-to-star variations in the light elements O and Na. These elements are known to vary, even to large extent, more than 1 dex, in GCs. This is possibly the main chemical signature of multiple populations and is visible only in massive and old stellar clusters. The lower limit in age is still debated; using results mainly based on nitrogen variations, which have an effect detectable also with photometry, there seems to be a convergence on 2 Gyr (see for instance Martocchia et al. 2019). However, Cadelano et al. 2022 found photometric indications of multiple populations on the MS of a 1.5 Gyr old clusters (but, interestingly, not among the red giants, possibly due to mixing). This indicates that the coordinated variations between light elements are not limited to the early Universe conditions. Mass and age seem to play an important role in determining whether multiple populations appear and it is not simple to disentangle their effects, meaning that it is interesting studying (also) younger and less massive clusters to constrain models. In summary, light elements variations are present in all MW GCs studied to date (with the possible exception of Rup 106) and in many massive clusters in the Magellanic Clouds and beyond. On the contrary, they have not been found in OCs (MacLean et al. 2015, see Pancino 2018 for an alternative view) when studied with large enough samples to understand whether an extended star formation process is required.

Keeping in mind the complications due to the different mass and age regimes of GCs and OCs, we studied the second in this work. *Gaia*-ESO is presently the best available source of data since it contains a large number of OCs (more than 80, combining GES proper and archive spectra) and large samples of stars in each of them. Unfortunately, Na and O are available only for the stars observed with UVES, since no lines of these elements are present in the GIRAFFE setups employed. Despite this limitation, GES constitutes the largest database we can tap for our study.

We used the public, final data release (see Sect. 1 for the location in the ESO catalogue archive). We selected stars belonging to OCs according to literature astrometry. After a further selection on errors, we ended up with 735 stars in 84 OCs (only 74 with at least three stars). Only part of the OCs have both Na and O abundance available, all have at least Na.

We then checked the Na-O distribution, finding no indication of an anti-correlation similar to that seen in GCs (we used the GC 47 Tuc as a comparison, as it has been analysed homogeneously by GES). Either the dispersion is compatible with being due to errors, or we see a correlation, contrary to what we see in GCs. We also checked the distribution of Na abundances alone, which was available for more stars and for different clusters. Also in this case, no unexplained dispersion was found. The few cases showing larger differences can be explained by evolutionary effects (i.e. differences between dwarfs and giants post first dredge-up) or by analysis problems.

Based on these results, OCs are simple stellar populations. Further steps to fully ascertain this, or finding that also these stellar clusters show ‘anomalous’ abundances and have populations distinct by their chemistry, comprise the following. Firstly, collecting larger samples of OCs where all light elements involved in (anti-)correlations in GCs can be measured, that is C, N, O, Na, Al, and Mg. This will be possible with large surveys such as WEAVE and 4MOST, where OCs are part of the scientific targets (see Jin et al. 2023; Lucatello et al. 2023), but

also GALAH and APOGEE (and its successor SDSS V) can contribute, as seen from the example at the end of Sect. 3.2. Secondly, collecting a large sample of stars in each cluster, as GES did. Thirdly, analysing samples in the most precise and homogeneous way possible, taking into account also evolutionary processes (diffusion, mixing, etc). The next step is checking the possible influence of rotation and binarity on the derived abundances; and, finally, taking into account departure from LTE for all elements involved, in particular Na.

More data on stellar clusters of all kinds will hopefully come from large surveys that are due to start soon, namely, WEAVE and 4MOST, to fully understand the nature of OCs. Both surveys have a low-resolution mode (about 5000) essentially covering the optical part of the spectra and a high-resolution mode (about 20000) covering three broad wavelength ranges. The latter mode, in particular, contains lines of O (the forbidden lines) and Na.

Acknowledgements. AB thanks Eugenio Carretta for useful comments on the manuscript. We thank the referee for useful comments which improved the paper presentation. This research has made use of the services of the ESO Science Archive Facility. This research has made use of the SIMBAD database (Wenger et al. 2000), operated at CDS, Strasbourg, France and of the VizieR catalogue access tool, CDS, Strasbourg, France (DOI: 10.26093/cds/vizieR). The original description of the VizieR service was published in Ochsenbein et al. (2000). This research has made use of NASA’s Astrophysics Data System. We made extensive use of TOPCAT (http://www.starlink.ac.uk/topcat/, Taylor 2005). This work has made use of data from the European Space Agency (ESA) mission *Gaia* (https://www.cosmos.esa.int/gaia), processed by the *Gaia* Data Processing and Analysis Consortium (DPAC, https://www.cosmos.esa.int/web/gaia/dpac/consortium). Funding for the DPAC has been provided by national institutions, in particular the institutions participating in the *Gaia* Multilateral Agreement. These data products have been processed by the FLAMES/UVES reduction team at INAF/Osservatorio Astrofisico di Arcetri. We acknowledge the support from INAF and Ministero dell’Istruzione, dell’Università e della Ricerca (MIUR) in the form of the grant Premiale VLT 2012 and Premiale 2016 MITiC. TB was funded by grant No. 2018-04857 from The Swedish Research Council

References

- Almeida, A., Monteiro, H., & Dias, W. S. 2023, MNRAS, 525, 2315
 Alonso-Santiago, J., Frasca, A., Catanzaro, G., et al. 2021, A&A, 656, A149
 Asplund, M., Grevesse, N., Sauval, A. J., Allende Prieto, C., & Kiselman, D. 2004, A&A, 417, 751
 Bastian, N. & Lardo, C. 2018, ARA&A, 56, 83
 Baumgardt, H. & Hilker, M. 2018, MNRAS, 478, 1520
 Bragaglia, A., Alfaro, E. J., Flaccomio, E., et al. 2022, A&A, 659, A200
 Bragaglia, A., Gratton, R. G., Carretta, E., et al. 2012, A&A, 548, A122
 Bragaglia, A., Sneden, C., Carretta, E., et al. 2014, ApJ, 796, 68
 Cadelano, M., Dalessandro, E., Salaris, M., et al. 2022, ApJ, 924, L2
 Cantat-Gaudin, T., Anders, F., Castro-Ginard, A., et al. 2020, A&A, 640, A1
 Carretta, E., Bragaglia, A., Gratton, R., D’Orazi, V., & Lucatello, S. 2011, A&A, 535, A121
 Carretta, E., Bragaglia, A., Gratton, R., & Lucatello, S. 2009a, A&A, 505, 139
 Carretta, E., Bragaglia, A., Gratton, R. G., et al. 2009b, A&A, 505, 117
 Carretta, E., Bragaglia, A., Gratton, R. G., et al. 2010, A&A, 516, A55
 Dekker, H., D’Odorico, S., Kaufner, A., Delabre, B., & Kotzlowski, H. 2000, in Society of Photo-Optical Instrumentation Engineers (SPIE) Conference Series, Vol. 4008, Optical and IR Telescope Instrumentation and Detectors, ed. M. Iye & A. F. Moorwood, 534–545
 Ebrahimi, H., Sollima, A., & Hathi, H. 2022, MNRAS, 516, 5637
 Freljij, H., Villanova, S., Muñoz, C., & Fernández-Trincado, J. G. 2021, MNRAS, 503, 867
 Gaia Collaboration, Brown, A. G. A., Vallenari, A., et al. 2021, A&A, 650, C3
 Gaia Collaboration, Vallenari, A., Brown, A. G. A., et al. 2023, A&A, 674, A1
 Gilmore, G., Randich, S., Worley, C. C., et al. 2022, A&A, 666, A120
 Gratton, R., Bragaglia, A., Carretta, E., et al. 2019, A&A Rev., 27, 8
 Gratton, R. G., Bonifacio, P., Bragaglia, A., et al. 2001, A&A, 369, 87
 Gratton, R. G., Carretta, E., & Bragaglia, A. 2012, A&A Rev., 20, 50
 Gratton, R. G., Sneden, C., Carretta, E., & Bragaglia, A. 2000, A&A, 354, 169
 Jackson, R. J., Jeffries, R. D., Wright, N. J., et al. 2022, MNRAS, 509, 1664
 Jin, S., Trager, S. C., Dalton, G. B., et al. 2023, MNRAS[arXiv:2212.03981]

- Kounkel, M. & Covey, K. 2019, *AJ*, 158, 122
- Kraft, R. P., Sneden, C., Langer, G. E., & Shetrone, M. D. 1993, *AJ*, 106, 1490
- Kruijssen, J. M. D., Pfeffer, J. L., Reina-Campos, M., Crain, R. A., & Bastian, N. 2019, *MNRAS*, 486, 3180
- Lagarde, N., Decressin, T., Charbonnel, C., et al. 2012, *A&A*, 543, A108
- Loaiza-Tacuri, V., Cunha, K., Souto, D., et al. 2023, *MNRAS*, 526, 2378
- Lucatello, S., Bragaglia, A., Vallenari, A., et al. 2023, *The Messenger*, 190, 13
- MacLean, B. T., De Silva, G. M., & Lattanzio, J. 2015, *MNRAS*, 446, 3556
- Magrini, L., Viscasillas Vázquez, C., Spina, L., et al. 2023, *A&A*, 669, A119
- Martocchia, S., Dalessandro, E., Lardo, C., et al. 2019, *MNRAS*, 487, 5324
- Mermilliod, J. C., Mayor, M., & Udry, S. 2008, *A&A*, 485, 303
- Milone, A. P., Piotto, G., Renzini, A., et al. 2017, *MNRAS*, 464, 3636
- Monelli, M., Milone, A. P., Stetson, P. B., et al. 2013, *MNRAS*, 431, 2126
- Mucciarelli, A., Bellazzini, M., Ibata, R., et al. 2012, *MNRAS*, 426, 2889
- Mucciarelli, A., Origlia, L., Ferraro, F. R., & Pancino, E. 2009, *ApJ*, 695, L134
- Ochsenbein, F., Bauer, P., & Marcout, J. 2000, *A&AS*, 143, 23
- Oh, W. S., Nordlander, T., Da Costa, G. S., Bessell, M. S., & Mackey, A. D. 2023, *MNRAS*, 524, 577
- Pancino, E. 2018, *A&A*, 614, A80
- Pancino, E., Lardo, C., Altavilla, G., et al. 2017a, *A&A*, 598, A5
- Pancino, E., Romano, D., Tang, B., et al. 2017b, *A&A*, 601, A112
- Pasquini, L., Avila, G., Blecha, A., et al. 2002, *The Messenger*, 110, 1
- Randich, S., Gilmore, G., Magrini, L., et al. 2022, *A&A*, 666, A121
- Renzini, A. & Fusi Pecci, F. 1988, *ARA&A*, 26, 199
- Sacco, G. G., Morbidelli, L., Franciosini, E., et al. 2014, *A&A*, 565, A113
- Smiljanic, R., Donati, P., Bragaglia, A., Lemasle, B., & Romano, D. 2018, *A&A*, 616, A112
- Smiljanic, R., Korn, A. J., Bergemann, M., et al. 2014, *A&A*, 570, A122
- Smiljanic, R., Romano, D., Bragaglia, A., et al. 2016, *A&A*, 589, A115
- Smith, G. H. & Norris, J. E. 1993, *AJ*, 105, 173
- Tarricq, Y., Soubiran, C., Casamiquela, L., et al. 2021, *A&A*, 647, A19
- Taylor, M. B. 2005, in *Astronomical Society of the Pacific Conference Series*, Vol. 347, *Astronomical Data Analysis Software and Systems XIV*, ed. P. Shopbell, M. Britton, & R. Ebert, 29
- Villanova, S., Carraro, G., Geisler, D., Monaco, L., & Assmann, P. 2018, *ApJ*, 867, 34
- Wenger, M., Ochsenbein, F., Egret, D., et al. 2000, *A&AS*, 143, 9
- Worley, C. C., Smiljanic, R., Magrini, L., et al. 2024, *A&A*, 684, A148

Appendix A: Supplementary information

We present some supplementary information on the OCs studied here, on the individual stars, and on a comparison of RV values with GDR3 results.

Appendix A.1: Literature information on the GES OCs

Table A.1 gives information on the OCs observed by GES, taken from literature: Nobs is the number of member stars observed with UVES; absorption in V , distance in pc, $\log \text{Age}$ (A_V , dist, logt) are taken from Cantat-Gaudin et al. (2020), with a few exceptions (NGC 6530, Cha I, ρ Oph, and γ Vel) taken from Randich et al. (2022); average cluster RV, standard error, and number of members used to derive them come from Tarricq et al. (2021); Y/N indicate whether oxygen was measured in the cluster; masses for part of the OCs are taken from Ebrahimi et al. (2022); Almeida et al. (2023); finally, some alternative names are given in last column (the names indicated by [KC2019] refer to Kounkel & Covey 2019).

Appendix A.2: Using [O/Fe] and [Na/Fe]

As commented in the main text, using the iron-scaled abundances risks introducing some spurious effects due to the existence of trends of [Fe/H] with temperature and $\log g$ (the topic is discussed in Magrini et al. 2023). However, even when we use [O/Fe] and [Na/Fe] (adopting 8.70 and 6.18 as solar abundances for O and Na, respectively), results are not changed from what we see for [O/H] and [Na/H].

Figure A.1 shows the stars in the O-Na plane (analogous to Fig. 1). In the right-most lower panel we see that essentially all OC stars have a [Na/Fe] level similar to stars of first generation in 47 Tuc.

Figure A.2 shows the histograms for [Na/Fe] (to be compared to Fig. 2). Again, we see that OC stars occupy the low-Na part of the distribution for the GC.

Finally, Fig. A.3 shows the average [Na/Fe] values for the OCs (with standard deviation indicated by error bars) as a function of metallicity. This distribution has to be compared to the individual stars in the GES catalogue and not belonging to OCs, to which we applied the same quality cuts (see Sect. 2). The GC 47 Tuc is shown for comparison, as done throughout the paper.

Appendix A.3: The individual stars

Table A.2 gives information on the individual stars, taken from GES and *Gaia* DR3. In particular, we list: name of the cluster, *Gaia* DR3 identification, GES object name, GES RV and error, T_{eff} and error, $\log g$ and error, metallicity, Na and O abundance with their errors, and *Gaia* DR3 RV with error. Only some of the first and last lines are shown here, the complete table is available at the CDS.

Appendix A.4: Comparison of GES and *Gaia* RVs

We checked the difference between GDR3 and GES velocities. The average difference, based on 578 stars, is 0.33 ($\sigma=7.00$) km s^{-1} , with values from about -70 to $+50$ km s^{-1} . The 535 stars with a ΔRV within 1σ have an offset of 0.22 ($\sigma=2.01$) km s^{-1} . Figure A.4 shows the ΔRV (in the sense GES-GDR3) and the

candidate binaries (those with $\Delta \text{RV} > 1\sigma$) are indicated by open blue circles.

The 43 candidate binaries are listed in Table A.3, where (after the name of the OC), we list the information from GDR3: the GDR3 identifier, RV, error, and number of transits used for the mean value, V_{broad} (a proxy for rotation velocity) and error when available, and the renormalised unit weight error (RUWE); finally, from the GES, RV and error, the membership probability, according to Cantat-Gaudin et al. 2020 and Jackson et al. 2022, and the ΔRV .

We note that besides the significant ΔRV , the large GDR3 errors on *Gaia* RVS radial velocity are already a strong indication of binarity. This is especially true when a large number of transits is available for the stars. For some of the stars, this is reinforced also by a RUWE larger than 1.4, which is indicative of a non-single star *Gaia* Collaboration et al. (2021); however, the RUWE does not intercept all binaries.

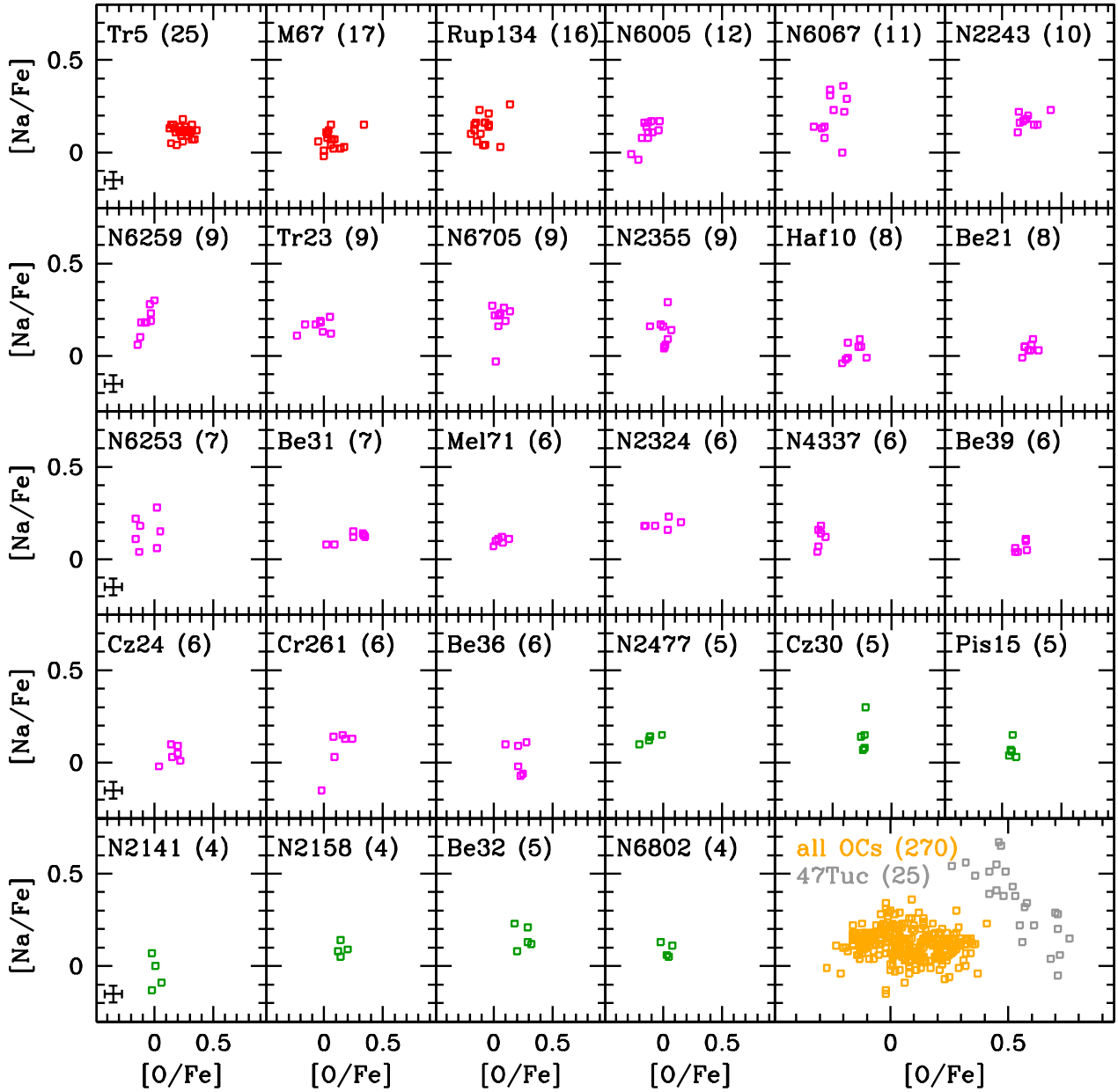


Fig. A.1. Distribution of $[Na/Fe]$ versus $[O/Na]$ for all OCs with at least four stars with valid values. The bottom-right panel displays the available values in all OCs (in orange) compared to the GC NGC 104/47 Tuc (grey points). The colours indicate clusters with more than 15 stars (red), 5-15 (magenta), and 4 (green).

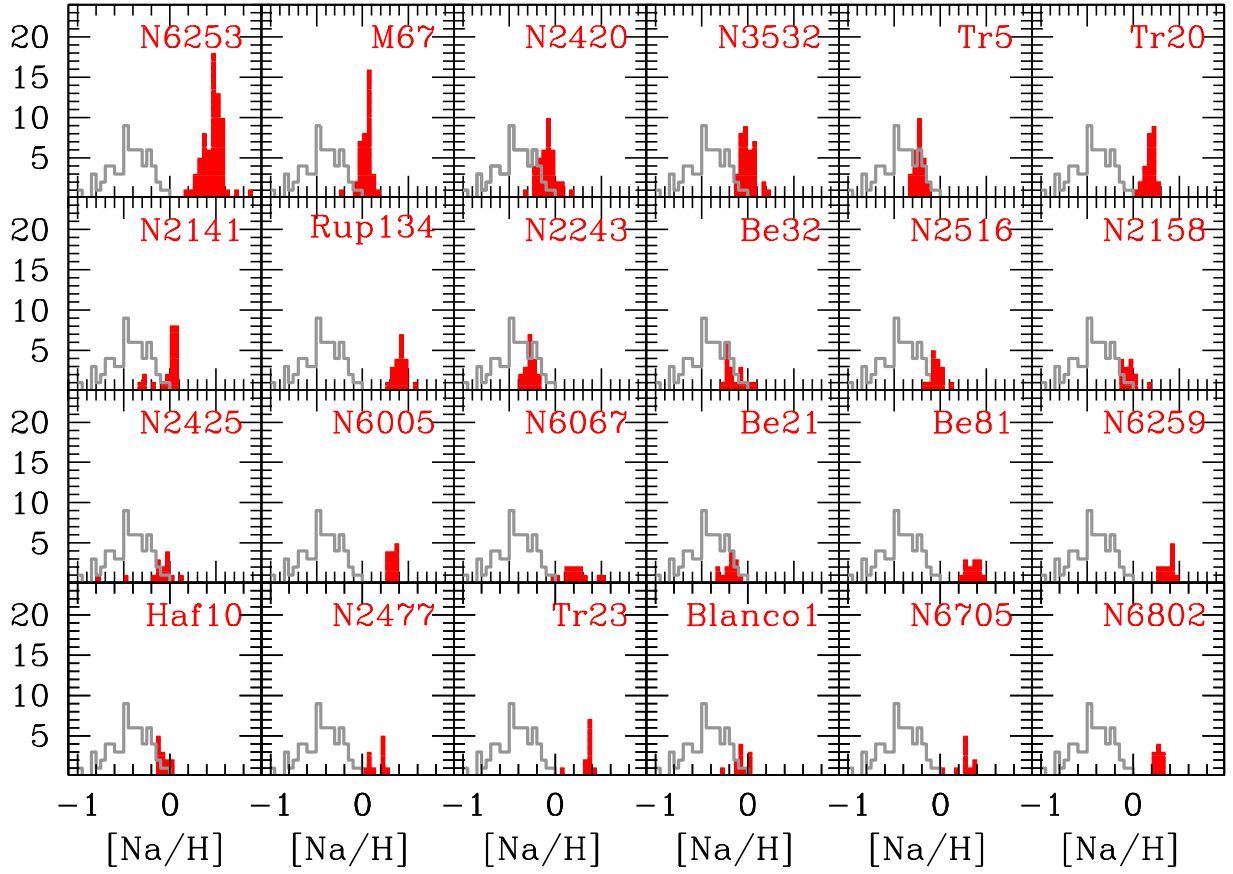


Fig. A.2. Histogram of $[\text{Na}/\text{Fe}]$ or all OCs with at least ten stars with valid values (filled red histograms). The histogram for NGC 104/47 Tuc (grey empty histogram) is also shown in each panel for comparison.

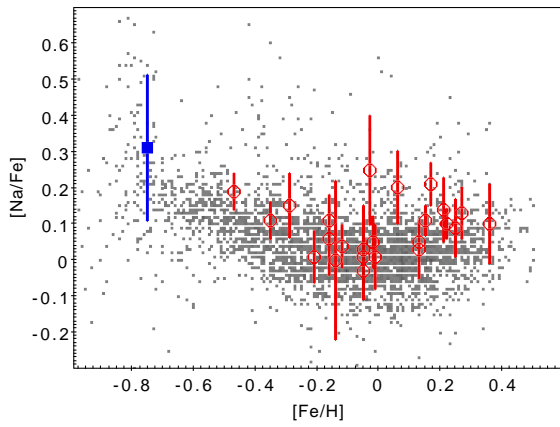


Fig. A.3. Plot of average $[Na/Fe]$ as function of $[Fe/H]$ for OCs (red circles, with error bars indicating the standard deviation). The small grey symbols are stars not in OCs (with the same quality cuts on $[Fe/H]$, T_{eff} , and $\log g$ applied to OCs). The GC 47 Tuc is also shown for comparison as a blue filled square.

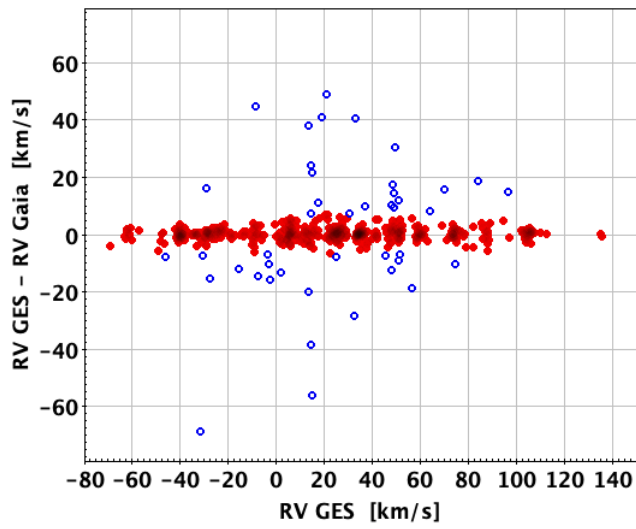


Fig. A.4. Difference in RV between GES and GDR3 values. The blue open circles indicate the candidate binary systems.

Table A.1. Literature information on the observed clusters.

Cluster	Nobs	A_V (mag)	dist (pc)	logt (yr)	logMass (M_\odot)	RV (km s^{-1})	stderr	N	O?	Alternative name (from Simbad)
NGC 6253	73	0.78	1653	9.51	3.457 ²	-24.48	0.19	249	Y	Mel 156
NGC 3532	43	0.00	498	8.60		+5.67	0.19	664	Y	[KC2019] Theia 720
M67	40	0.07	889	9.63	3.266 ²	+34.18	0.14	360	Y	NGC 2682
NGC 2420	37	0.04	2587	9.24		+74.78	0.09	326	N	Cr 154, Mel 69
NGC 6705	35	1.20	2203	8.49		+34.49	0.27	357	Y	M11, Cr 391, Mel 213
NGC 2547	29	0.14	396	7.51	2.559 ² ,2.517 ¹	+13.05	0.16	134	N	[KC2019] Theia 74
NGC 2516	28	0.11	423	8.38	3.296 ¹	+24.24	0.07	490	N	[KC2019] Theia 613
NGC 2264	27	0.79	707	7.44	2.566 ²	+22.54	0.26	141	Y	[KC2019] Theia 41
Trumpler 5	26	1.20	3047	9.63		-23.10	0.19	5	Y	Cr 105
Trumpler 20	26	0.88	3392	9.27		-39.85	0.18	430	Y	
NGC 2141	23	0.97	5183	9.27		+27.11	0.23	429	Y	Cr 79
Berkeley 39	23	0.29	3968	9.75		+59.41	0.14	394	Y	
Ruprecht 134	20	1.15	2252	9.22		-39.47	0.63	72	Y	
NGC 6067	20	0.97	1881	8.10		-38.01	0.50	256	Y	Mel 140
NGC 2243	19	0.02	3719	9.64		+60.02	0.10	356	Y	Mel 46
IC 2602	18	0.02	149	7.56	2.442 ² ,2.236 ¹	+17.60	0.12	76	Y	Cr 229, Mel 102, [KC2019] Theia 92
Berkeley 32	17	0.34	3072	9.69		+105.68	0.41	202	Y	Biurakan 8
NGC 6530	16		1325	6.30					N	
Blanco 1	16	0.01	240	8.02	2.529 ² ,2.594 ¹	+6.23	0.07	172	Y	
NGC 2451A	5	0.00	195	7.55	2.534 ² ,2.418 ¹	+23.42	0.13	70	N	[KC2019] Theia 118
NGC 2451B	10	0.18	361	7.61	2.565 ²	+15.23	0.09	75	N	
IC 2391	14	0.04	148	7.46	2.332 ² ,2.207 ¹	+15.58	0.48	67	N	o Vel Cluster, [KC2019] Theia 114
NGC 2158	14	1.44	4298	9.19		+27.15	0.18	284	Y	Mel 40
NGC 2425	14	0.89	3576	9.38		+102.36	0.60	132	Y	
NGC 6005	13	1.42	2383	9.10		-22.65	0.75	86	Y	Mel 138
NGC 6259	13	1.87	2314	8.43		-32.12	1.20	125	Y	
Berkeley 21	13	1.96	6417	9.33		+4.84	1.45	57	Y	
Berkeley 81	13	2.75	3313	9.06	3.295 ²	+45.92	0.99	64	Y	
IC 4665	12	0.45	354	7.52	2.489 ²	-13.31	0.37	47	N	Cr 349, Mel 179, [KC2019] Theia 96
Chamaleon I	12		189	6.20					N	
Haffner 10	12	1.35	3409	9.58		+87.97	0.32	87	Y	
NGC 2477	11	0.68	1442	9.05		+8.46	0.10	197	Y	Mel 78
Trumpler 14	11	1.00	2290	7.80	3.300 ²	-10.01	2.53	79	N	
Trumpler 23	11	2.18	2590	8.85		-63.75	1.57	79	Y	
NGC 6802	10	2.37	2753	8.82		+10.31	1.30	100	Y	Cr 400
NGC 2355	9	0.59	1941	9.00	2.848 ²	+36.37	0.26	118	Y	Cr 133, Mel 63
Melotte 71	9	0.38	2139	8.99		+50.98	0.34	108	Y	Cr 155
λ Ori	9	0.25	416	7.10		+27.73	0.13	285	N	Collinder 69, Briceno 1, MWSC 0531
Berkeley 31	9	0.35	7177	9.45		+61.39	1.25	77	Y	Biurakan 7
Tombaugh 2	9	0.83	9316	9.21		+122.47	0.40	11	Y	Haffner 2
NGC 2324	8	0.40	4214	8.73		+47.09	1.34	14	Y	Mel 59
NGC 6405	8	0.49	459	7.54		-7.42	0.41	124	N	M38, M43, [KC2019] Theia 122
NGC 6791	8	0.70	4231	9.80		-47.75	0.17	57	N	Be 46
ASCC 50	8	0.99	917	7.06		+21.44	0.26	158	N	Alessi 43
NGC 6281	7	0.30	539	8.71		-5.05	0.39	77	Y	[KC2019] Theia 325
NGC 6633	7	0.30	424	8.84	2.709 ⁷	-29.10	1.07	72	Y	[KC2019] Theia 924
Berkeley 22	7	1.99	6225	9.39		+94.31	0.44	17	N	
Berkeley 44	7	2.75	2863	9.16		-7.54	0.58	41	N	
Czernik 30	7	0.62	6647	9.46		+82.07	0.73	46	Y	
NGC 4337	7	1.06	2450	9.16	3.021 ²	-17.26	0.29	19	Y	
NGC 4815	6	1.75	3295	8.57		-28.11	1.09	83	Y	
Pismis 15	6	1.89	2599	8.94	2.744 ²	+34.22	0.94	53	Y	
Pismis 18	6	1.81	2860	8.76		-24.85	0.89	42	Y	IC 4291
Berkeley 36	6	1.42	4360	9.83		+62.94	0.25	112	Y	
Czernik 24	6	1.63	3981	9.43		+21.52	0.48	71	Y	
Collinder 261	6	0.81	2850	9.80		-24.43	0.17	230	Y	Harward 6
NGC 2232	5	0.01	315	7.25	2.356 ² ,2.281 ¹	+25.75	0.11	69	Y	[KC2019] Theia 55
NGC 2660	5	1.19	2788	8.97		+22.47	0.27	8	Y	Mel 92
Berkeley 25	5	1.07	6780	9.39		+108.07	9.19	14	N	

Table A.1. continued.

Cluster	Nobs	A_V (mag)	dist (pc)	logt (yr)	logMass (M_\odot)	RV (km s^{-1})	stderr	N	O?	Alternative Name (from Simbad)
Ruprecht 7	5	1.75	5851	8.37		+77.38	0.32	7	Y	Berkeley 33
25 Ori	5	0.25	416	7.10		+27.73	0.13	285	N	Collinder 69
Collinder 110	5	1.14	2183	9.26		+38.15	0.21	48	Y	
Ruprecht 147	4	0.06	323	9.48		+42.18	0.38	99	Y	NGC 6774, [KC2019] Theia 1531
NGC 6192	4	1.57	1737	8.38	3.265 ²	-7.71	0.19	6	Y	Cr 309
NGC 6709	4	0.72	1041	8.28	2.832 ²	-4.22	1.09	91	Y	[KC2019] Theia 985
ρ Oph	4		139	5.5-6.8						N
ESO092-05	4	0.17	12444	9.65		+57.40	3.38	22	N	
Berkeley 30	4	1.27	5383	8.47	2.959 ²	+46.94	0.84	53	Y	Biurakan 9
Berkeley 73	4	0.69	6158	9.15		+97.51	0.53	28	N	
Berkeley 75	4	0.29	8304	9.23		+122.41	1.73	23	Y	ESO490-50
NGC 3293	3	0.90	2710	7.01	3.296 ²	-7.04	3.37	25	N	Cr 224, Mel 100
NGC 3766	3	0.66	2123	7.36		-16.18	0.59	21	N	Cr 248
NGC 6583	3	1.52	2053	9.08		-1.43	0.49	34	Y	
γ Vel	3		330	7.30						N
NGC 5822	2	0.39	854	8.96		-28.71	0.14	39	N	Mel 130,[KC2019] Theia 1174
Berkeley 20	2	0.37	8728	9.68		+75.65	1.38	3	Y	
Berkeley 29	2	0.24	12604	9.49		+25.72	1.99	9	Y	
Ruprecht 4	2	1.24	4087	8.93	2.868 ²					Y
Collinder 197	2	1.42	955	7.15		+28.84	0.50	101	N	ESO313-13, [KC2019] Theia 28
NGC 2244	1	1.46	1478	7.10		+32.86	1.00	142	N	NGC 2239
NGC 6404	1	3.47	2500	8.00		+10.12	0.26	9	N	
NGC 6649	1	3.90	2124	7.85		+4.50	1.09	86	N	

Notes: ¹ Ebrahimi et al. (2022); ² Almeida et al. (2023)

Table A.2. Properties of the individual stars (excerpt).

Cluster	DR3 ID Gaia	object GES	RV GES	err	T_{eff} GES	err	$\log g$ GES	err	[Fe/H] GES	err	NaI GES	err	O1 GES	err	RV Gaia	err
25 Ori	3222177030594592256	05233297+0135176	14.41	0.37	6568	39	4.06	0.07	-0.07	0.05	6.24	0.14			17.27	1.84
lamOri	3339510731055206528	05352469+1011453	29.33	0.37	6200	37	4.16	0.07	-0.06	0.05	6.12	0.05			29.67	0.72
lamOri	3337936092965373568	05361858+0945089	29.06	0.37	5040	35	4.42	0.05	-0.10	0.05	6.33	0.14			27.62	4.73
lamOri	3336149489649827840	05432474+0906084	25.01	0.37	4542	30	4.10	0.05	-0.18	0.05	5.96	0.05			23.95	15.75
Blanco1	2320833372790628480	00013320-3012597	6.59	0.37	5311	31	4.55	0.05	-0.05	0.05	6.03	0.02			7.33	1.11
Blanco1	2333005344467248768	00024879-2918422	5.69	0.37	5446	31	4.42	0.05	-0.02	0.05	6.08	0.02			5.03	1.07
Blanco1	2320795340855502336	00023546-3007019	-3.27	0.37	5303	30	4.50	0.05	-0.09	0.05	5.91	0.05			7.06	3.17
Blanco1	2320795237776344704	00030028-3003216	6.52	0.37	5017	31	4.48	0.05	-0.07	0.05	6.19	0.02			5.94	1.55
Blanco1	2320869901488170624	00032061-2949227	5.58	0.37	6230	32	4.36	0.05	-0.05	0.05	6.19	0.06			5.67	0.61
Blanco1	2320591205353715712	00050824-3029421	6.04	0.37	5754	32	4.42	0.05	0.01	0.05	6.15	0.02			5.36	0.58
Blanco1	2320925564263593088	00043317-2938281	5.47	0.37	6317	33	4.18	0.05	-0.03	0.05	6.09	0.05			5.81	0.64
Blanco1	2320916768170630912	00055905-2939046	5.41	0.37	5923	36	4.47	0.05	-0.01	0.05	6.11	0.14			5.66	1.43
Blanco1	2320617529209321728	00045884-3009416	5.93	0.37	6038	44	4.34	0.09	-0.12	0.08	6.20	0.12			5.77	0.67
Blanco1	2320617116892496256	00052902-3008321	8.58	0.37	4832	30	4.58	0.05	-0.07	0.05	6.07	0.02	9.00	0.10	5.84	1.96
Blanco1	2320615983021130752	00055472-3006258	6.02	0.37	5677	30	4.47	0.05	-0.01	0.05	6.12	0.05				
Be20	3221067898239847168	05323677+0011048	78.81	0.37	4847	31	2.70	0.05	-0.32	0.06	6.04	0.02	8.66	0.15		
Be20	3221067902536353152	05323896+0011203	78.91	0.37	4382	31	1.81	0.06	-0.43	0.06	5.92	0.05	8.54	0.10	83.45	3.97
Be21	3424170411975583616	05513844+2147197	0.72	0.37	4368	33	1.80	0.06	-0.26	0.04	5.91	0.02	8.61	0.12	1.25	2.82
Be21	3424170549414520832	05514200+2148497	-0.46	0.37	4520	33	2.25	0.05	-0.18	0.04	6.09	0.02	8.78	0.15	-4.21	4.44
Be21	3424170515054788736	05514204+2148027	0.91	0.37	4509	31	2.15	0.05	-0.23	0.05	5.98	0.05	8.71	0.15	1.66	3.21
....																
Trumpler23	5980830577767550976	16010639-5331056	-62.41	0.37	4725	33	2.63	0.05	0.15	0.04	6.52	0.05	8.82	0.07	-63.63	1.06
Trumpler23	5980841916481958144	16003935-5332367	-61.36	0.37	4725	33	2.63	0.05	0.18	0.04	6.57	0.05	8.93	0.05	-60.93	0.70
Trumpler23	5980842431878045696	16004312-5330509	-62.22	0.37	4815	33	2.85	0.05	0.24	0.04	6.53	0.05	8.71	0.07	-63.99	2.32
Trumpler23	5980830607806894720	16005168-5332013	-63.26	0.37	4784	33	2.60	0.05	0.21	0.04	6.57	0.05	8.88	0.05	-62.63	0.83
Trumpler23	5980830405968813824	16010025-5333101	-60.66	0.37	4805	33	2.72	0.05	0.20	0.04	6.55	0.05	8.74	0.07	-62.85	1.31
Trumpler23	5980832055236335744	16010770-5329374	-61.94	0.37	4753	32	2.63	0.05	0.22	0.04	6.57	0.05	8.85	0.06	-63.70	0.83
Trumpler23	5980842500597538304	16004025-5329439	-56.95	0.37	4765	33	2.68	0.05	0.19	0.04	6.56	0.05			-58.23	2.67
Trumpler23	5980841916481954432	16004035-5333047	-69.15	0.37	4768	33	2.96	0.05	0.03	0.04	6.27	0.04			-65.34	0.82
Trumpler23	5980830199810393216	16005220-5333362	-62.92	0.37	4817	32	2.65	0.05	0.26	0.05	6.62	0.05	8.93	0.04	-61.41	3.03
Trumpler23	5980830646487029248	16005798-5331476	-60.43	0.37	4767	32	2.70	0.05	0.23	0.04	6.54	0.05	8.92	0.04	-58.49	1.17

Table A.3. Candidate binaries on the basis of the RV difference between *Gaia* DR3 and GES.

Cluster	Gaia DR3 ID	RV (GDR3)	err	num	Vbroad (GDR3)	err	RUWE	RV (GES)	err	proba	mem3d	ΔRV
Blanco 1	2320795340855502336	7.06	3.17	19			7.699	-3.270	0.37		0.95	-10.33
Be 21	3424170549414515200	3.62	1.89	14			1.074	-3.430	0.38	0.8	1.00	-7.05
Be 31	3157239843797500672	75.13	8.60	8			0.995	56.600	0.37	0.9	1.00	-18.53
Be 36	3032952217629397760	55.90	6.66	10			1.056	63.920	0.37	1.0	1.00	8.02
Be 73	3007967052833159296	81.90	7.39	20			1.019	96.790	0.37	1.0	1.00	14.89
Be 81	4265584329578299904	39.32	4.44	12			0.952	48.900	0.37	1.0	1.00	9.58
Be 81	4265584054700298240	37.80	9.06	9			1.010	48.040	0.37	0.9	1.00	10.24
Be 81	4265582577231602304	30.92	12.62	6			0.956	48.440	0.37	1.0	1.00	17.52
Be 81	4265582405432857472	60.34	5.52	5			1.090	48.140	0.37	1.0	1.00	-12.20
Cha I	5225317513655541504	-9.76	6.78	25			25.026	14.430	0.37		1.00	24.19
Cha I	5201154444261256704	71.36	10.71	6			1.075	15.150	0.37		1.00	-56.21
Cha I	5201362423758639744	-6.59	13.19	16			1.136	15.140	0.38		1.00	21.73
IC 4665	4474066401451091840	6.59	7.70	19	39.42	29.36	0.939	17.590	0.37	1.0	0.95	11.00
M 67	604911410242410752	38.82	5.29	24			15.870	50.880	0.37		0.96	12.06
M 67	604922985178465152	34.60	2.26	25			1.373	49.260	0.37	1.0	0.99	14.66
M 67	604917629355038848	37.05	9.14	19			0.918	-31.680	0.37	0.8	1.00	-68.73
M 67	604917491916095872	52.81	9.52	19	16.31	20.02	0.942	14.400	0.37	0.8	0.99	-38.41
Mel 71	3033961638024647808	65.42	4.96	22			1.020	84.120	0.37	0.9		18.70
Mel 71	3033962050339630208	61.01	5.51	21	7.74	8.05	1.028	32.640	0.37	1.0		-28.37
Mel 71	3033958747506151424	53.10	3.87	26	10.56	17.82	0.941	45.700	0.37	1.0		-7.40
Mel 71	3033962187778553600	54.50	2.98	20	6.95	12.44	1.482	70.300	0.37	0.7		15.80
NGC 2264	3326929191297621120	-7.66	8.03	8			1.152	32.940	0.37	0.9	0.98	40.60
NGC 2264	3326904521005483136	33.12	4.64	9			0.921	25.160	0.37	0.9	0.98	-7.96
NGC 2264	3326685443313414144	-22.21	5.52	8			1.088	18.800	0.38		0.97	41.01
NGC 2264	3326696124896220928	-27.97	4.79	9			1.021	21.050	0.27		1.00	49.02
NGC 2420	865398496685953536	84.54	9.19	9			1.001	74.350	0.10	0.9	1.00	-10.19
NGC 2451	5538749417871537024	13.15	2.23	21	37.49	27.60	1.338	-2.720	0.37	0.9		-15.87
NGC 2451	5538817690669417984	7.20	4.76	16			1.649	14.610	0.38	0.8		7.41
NGC 2516	5290767115830162560	19.13	7.48	20			2.364	49.630	0.38	0.7	0.97	30.50
NGC 2547	5514369229297396736	-24.70	10.25	10			0.994	13.520	0.37	0.9	1.00	38.22
NGC 2547	5514371874997910656	33.46	5.67	7			4.536	13.640	0.37		1.00	-19.82
NGC 3532	5340146079993296384	6.88	3.03	15			2.920	-7.780	0.37		0.97	-14.66
NGC 3532	5340215349223412992	27.12	5.36	7			1.053	37.150	0.37	1.0	0.85	10.03
NGC 6253	5935992940300723072	-23.17	13.83	17			1.006	-30.630	0.37	0.8	1.00	-7.46
NGC 6253	5935943530992746880	-45.56	12.08	12			0.976	-29.260	0.37	0.8	1.00	16.30
NGC 6253	5935945180260232064	-12.45	17.47	10			1.010	-27.670	0.37		0.99	-15.22
NGC 6405	4054223731895900288	-53.44	4.78	15			0.855	-8.610	0.37	1.0	0.99	44.83
NGC 6530	4066064956700837248	-3.37	7.63	15	323.50	49.20	0.789	-15.510	1.60		0.92	-12.14
Pismis 15	5410176380718863232	23.13	2.53	24			1.034	30.680	0.37	1.0	0.99	7.55
Rup 134	4056457630330166784	-38.39	10.15	2			1.434	-45.950	0.37		0.96	-7.56
Trumpler 5	3326785773750746112	59.96	4.47	7			1.040	51.130	0.37	1.0	1.00	-8.83
Trumpler 5	3326786564024669696	58.16	5.52	10			0.957	51.340	0.37	1.0	1.00	-6.82
gamma Vel	5519267038205288832	14.89	4.90	15	76.91	35.31	0.998	1.720	0.37		0.88	-13.17